

Al³⁺ doped Fe₃O₄ Nanoparticles: A Novel Preparation Method, Structural, Magnetic and Electrochemical Characterizations

Mustafa Aghazadeh¹, Isa Karimzadeh², Mohammad Reza Ganjali^{3,4,*} and Ali Malekinezhad¹

¹ Materials and Nuclear Research School, Nuclear Science and Technology Research Institute (NSTRI), P.O. Box 14395-834, Tehran, Iran

² Department of Physics, Faculty of Science, Central Tehran Branch, Islamic Azad University, Tehran, Iran

³ Center of Excellence in Electrochemistry, School of Chemistry, College of Science, University of Tehran, Tehran, Iran

⁴ Biosensor Research Center, Endocrinology and Metabolism Molecular-Cellular Sciences Institute, Tehran University of Medical Sciences, Tehran, Iran

*E-mail: ganjali@khayam.ut.ac.ir

Received: 30 April 2017 / Accepted: 29 June 2017 / Published: 13 August 2017

Aluminum doped magnetite (Fe₃O₄) nanoparticles were synthesized through one-pot facile electrochemical method. In this method, products were electro-deposited on a stainless steel (316L) cathode from an additive-free 0.005M Fe(NO₃)₃/FeCl₂/AlCl₃ aqueous electrolyte. The structural characterizations through X-ray diffraction (XRD), field emission electron microscopy (FE-SEM) and energy-dispersive X-ray (EDX) indicated that the deposited material has Al doped magnetite particles with average size of 15 nm. Magnetic analysis by VSM showed the super-paramagnetic nature of the prepared nanoparticles ($M_s = 18.37 \text{ emu g}^{-1}$, $M_r = 0.13 \text{ emu g}^{-1}$, and $H_{Ci} = 8.73 \text{ G}$). The charge storage capability evaluation of the prepared nanoparticles through cyclic voltammetry (CV) and galvanostat charge-discharge (GCD) confirmed that these materials are capable to deliver specific capacitances as high as 236.1 F g^{-1} (at 0.2 A g^{-1}), and 180.2 F g^{-1} (at 1 A g^{-1}), and capacity retentions of 95.6% and 89.4% after 2000 cycling at 0.2 and 1 A g^{-1} , respectively. The results confirmed that the applicability of the electro-synthesized nanoparticles in supercapacitors. Besides, the study shows a simple electrochemical method for preparation of metal doped magnetite nanoparticles.

Keywords: Nanoparticles; Magnetite; Al doping; Cathodic electrosynthesis; Charge storage

1. INTRODUCTION

Supercapacitors, also called electrochemical capacitors, have attracted global attention because of their excellent energy storage capability for a variety of applications [1]. They supply energy

through ion adsorption at the electrode/electrolyte interface or based on faradic redox reactions by using high-energy electrode materials such as metal oxides, metal-doped carbons, or conductive polymers. Increasing attention has focused on the metal oxides and hydroxides with excellent electrochemical performance in recent years, which includes cobalt oxides [2-4], copper oxide [5], nickel oxide [6-8], MnMoO_4 [9], manganese oxides [10-15], cobalt hydroxides [16-22], nickel hydroxide [23-26], hematite [27-29] and magnetite [30-33]. Amongst these materials, iron oxides i.e. $\alpha\text{-Fe}_2\text{O}_3$ and Fe_3O_4 have concerned much attention due to their variable oxidation states, natural abundance, low cost, as well as the environmental friendliness [34]. However, the specific capacitance and high charge/discharge rates of different magnetite are considerably restricted due to the naturally low electrical conductivity, which hinders their extensive use in commercial supercapacitors [35,36]. To overcome these obstacles, a number of processes, include mixing with carbon-based material (i.e. graphene, carbon nanotubes,...) [37-40], doping with metal ions [41], and fabricating new nanostructures [42-45] have been applied. These works have proved that an improvement of charge storage ability of iron oxides can be achieved as results of enhancing the conductivity, increasing the surface area, shorten the diffusion paths and redox activity. Among these strategies, metal ion doping has been rarely investigated. In this paper, we introduced a novel method for preparation of metal ion (Al^{3+}) doped magnetite nanoparticles (Al-MNPs) based on the cathodic electrodeposition procedure. Notably, we recently found that the pure phase of Fe_3O_4 with fine sizes (10-15nm) can be easily synthesized through cathodic electrodeposition (CED) from additive-free aqueous solution of mixed iron (III)nitrate/iron(II) chloride [46-48]. Here, we applied a similar route for fabrication of Al-MNPs. To the best of our knowledge, the electrochemical synthesis of metal doped- Fe_3O_4 nanoparticles has not been reported until now. The prepared materials were determined by XRD, IR, FE-SEM, VSM, cyclic voltammetry (CV) and galvanostat charge-discharge (GCD) techniques. The results of these analyses confirmed the suitable magnetic and supercapacitive performance of Al-MNPs.

2. EXPERIMENTAL PROCEDURE

2.1. Materials

Ferrous chloride tetrahydrate ($\text{FeCl}_2 \cdot 4\text{H}_2\text{O}$, 99.5%), ferric nitrate nonahydrate ($\text{Fe}(\text{NO}_3)_3 \cdot 9\text{H}_2\text{O}$, 99.9%), Aluminum chloride ($\text{AlCl}_3 \cdot 6\text{H}_2\text{O}$, 99.5%) and polyvinylidene fluoride (PVDF, $(\text{CH}_2\text{CF}_2)_n$) were obtained from Sigma Aldrich. All chemicals were used as received.

2.2. Electrosynthesis of nanoparticles

The cathodic electrodeposition (CED) process previously reported for the synthesis of magnetite nanoparticles (MNPs) [48-50], was used for the preparation of Al-doped Fe_3O_4 nanoparticles. A schematic view of the synthesis procedure is presented in Fig. 1.

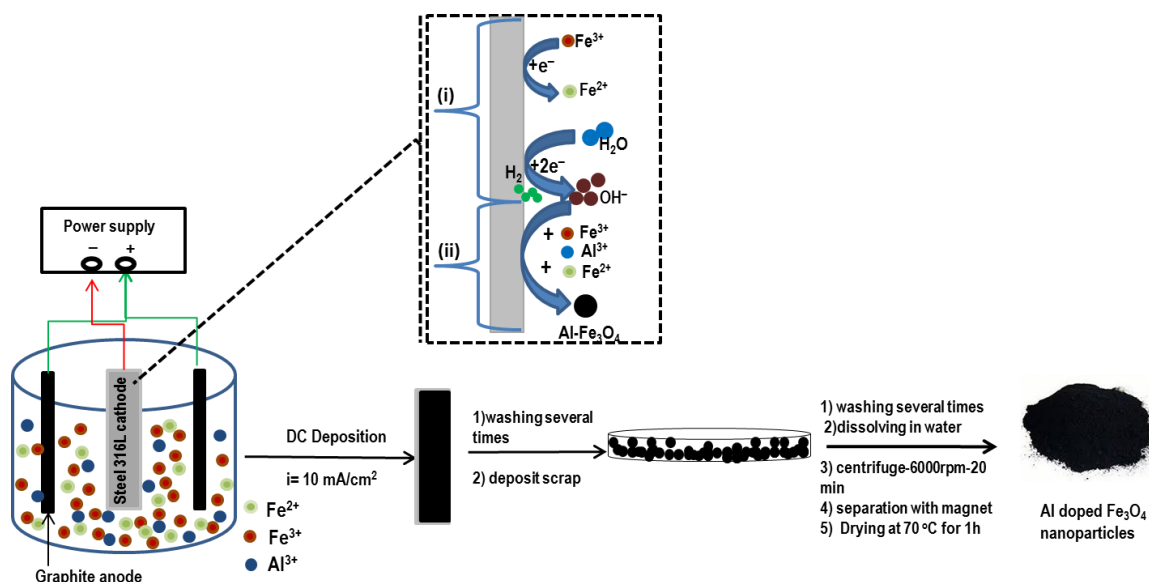


Figure 1. Schematic view of electrosynthesis of Al^{3+} doped Fe_3O_4 nanoparticles. The inset shows the electrochemical step (i) and chemical step (ii) of $\text{Al-Fe}_3\text{O}_4$ formation on the cathode surface.

The electrochemical cell contained a (316 L, $5\text{cm} \times 5\text{cm} \times 0.5\text{mm}$) stainless-steel which the cathode was placed between two parallel graphite anodes as seen in Fig. 1. An aqueous solution of $0.005\text{M Fe}(\text{NO}_3)_3 \cdot 9\text{H}_2\text{O}/\text{FeCl}_2 \cdot 4\text{H}_2\text{O}/\text{AlCl}_3 \cdot 6\text{H}_2\text{O}$ (2g:1g:0.4g) was used as the electrolyte. The deposition steps were done by an electrochemical workstation system (Potentiostat/Galvanostat, Model: NCF-PGS 2012, Iran) and the deposition was done at a current density of 10 mA cm^{-2} . 30 min is required for deposition and in 25°C bath. Next to the deposition process, the steel substrates were rinsed using deionized water for several times, and the deposit was scraped from the electrode surface and washed with water several times again, as noted in Fig. 1. Finally, the deposit was dispersed in deionized water and centrifuged at 6000rpm for 20min as indicated in Fig. 1. Subsequently, the deposit was separated from water using a magnet, then dried at 70°C for 1h, and the resultant black powder named Al-MNPs, and was used for next studies.

2.3. Characterization analyses

Morphology of the synthesized powder was observed by field-emission scanning electron microscopy (FE-SEM, Mira 3-XMU with accelerating voltage of 100 kV). Crystal structure of the powder was considered by X-ray diffraction (XRD, Phillips PW-1800) using a $\text{Co K}\alpha$ radiation. The FTIR spectra were obtained using a Bruker Vector 22 Fourier transformed infrared spectroscope. The magnetic properties of the prepared naked and coated NPs were assessed in the range of -20000 to 20000 Oe at room temperature by vibrational sample magnetometer (VSM, model: Meghnatis Daghigh Kavir, Iran).

2.4. Electrochemical studies

Cyclic voltammetry (CV) and galvanostatic charge–discharge (GCD) tests were done by a potentiostat (AUTOLAB[®], Eco Chemie, PGSTAT 30). A three-electrode set-up applied in the CV and GCD experiments was made of a working electrode (Al-Fe₃O₄ nanoparticles paste electrode), an Ag/AgCl reference electrode (saturated with 1 M KCl), and a counter electrode (platinum wire). All the electrochemical data were collected in a 1M Na₂SO₃ aqueous electrolyte. Al-MNPs working electrode (WE) was fabricated through a well-known method [51], according to which the prepared black Al-Fe₃O₄ powder was physically mixed with acetylene black (>99.9%) and conducting graphite (with ratios of 75:10:10), and the mixture was homogenized. Then, 5 wt.% polyvinylidene fluoride (PVDF) dissolved in N-Methyl-2-pyrrolidone (NMP) was added. After partially evaporating the NMP content of the mixture, the resulting paste was pressed at 10 MPa onto Ni foam (1 cm²). The assembled WE was dried for 5 min at about 150 °C in oven. The mass of the loaded Al-MNPs powder in the fabricated WE was about 3 mg. The CVs of the made WE were obtained in a 1M Na₂SO₃ solution in the potential window of -1.0 and +0.1 V vs. Ag/AgCl. The CV profiles were collected at the scan rates of 2, 5, 10, 20, 50 and 100 mV s⁻¹ and the SCs were obtained from the CV profiles by Eq. (1) [15,16]:

$$C = \frac{Q}{m \nu \Delta V}, \quad Q = \int_{V_a}^{V_b} I(V) dV \quad (1)$$

where C is the capacitance of the prepared powder (F g⁻¹), Q is the total charge, ΔV is the applied potential, m is the mass of Al-MNPs powder (g), ν is the scan rate (V s⁻¹) and I(V) is the current response during the potential scan. The GCD curves were recorded at the altered current loads of 0.5, 1, 2, 3 and 5 A g⁻¹ within a potential range of -1.0 to 0V vs. Ag/AgCl. The SCs of the fabricated WE were determined using following formula [27]:

$$C = \frac{Q}{m \times \Delta V}, \quad Q = I \times \Delta t \quad (2)$$

where C is the calculated capacitance for the WE, I is the applied current load (A), ΔV is the applied potential range (1V), Δt is the time of a discharge cycle (s) and m is the mass of Al-MNPs powder (g). Electrochemical impedance spectroscopy (EIS) measurements were done under the open circuit potential in an AC frequency range from 10⁵ to 10⁻² Hz with an excitation signal of 5 mV.

3. RESULTS AND DISCUSSION

3.1. Characterizations

Fig. 2 shows the XRD pattern of prepared powder. All the observed diffraction peaks in the XRD pattern could be readily identified as the pure cubic phase [space group: Fd3m (227)] of Fe₃O₄ with cell constants $a = 8.389 \text{ \AA}$ (JCPDS 01-074-1910). The absence of any extra peak other than Fe₃O₄ indicated that the electrodeposited product has pure phase. This implicates that the iron oxide is completely formed in the Fe₃O₄ phase on the cathode surface at our applied deposition conditions. The Al³⁺ cations played the same role of Fe³⁺ cations during the deposition time. And they occupied some site of the Fe³⁺ ions in the magnetite structure. As a results Al doped Fe₃O₄ is prepared as the

deposition product and its XRD pattern is completely fitted to the magnetite phase (Fig. 2). The average crystallite size (D) of the Al-MNPs was calculated using the Debye–Scherrer equation, $D=0.9\lambda/\beta\cos(\theta)$, where λ is the X-ray wavelength, β is the full width at half maximum of the diffraction line, and θ is the diffraction angle of the XRD pattern. From the diffraction line-width of (311) peak, the average crystallite size of the prepared MNPs was calculated to be 14.8 nm.

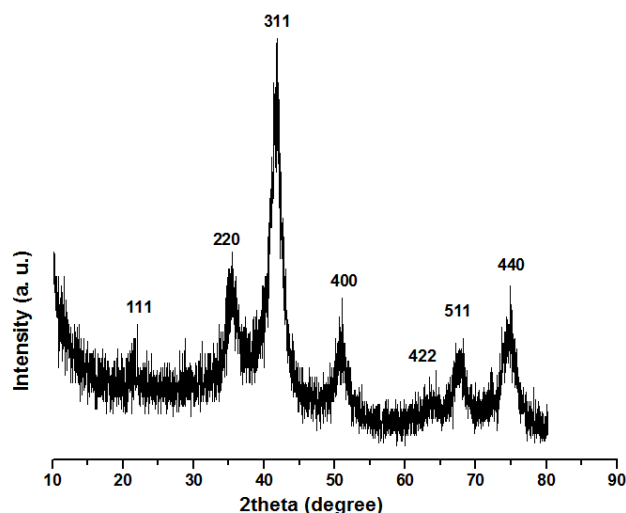


Figure 2. XRD pattern of the electro-synthesized Al doped magnetite nanoparticles.

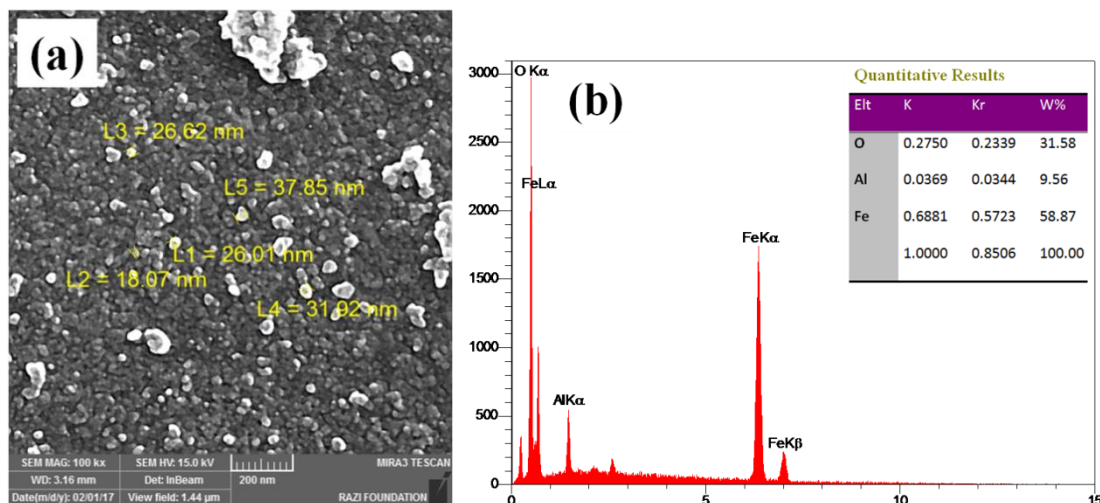


Figure 3. (a) FE-SEM and (b) EDS analysis of the prepared Al doped magnetite nanoparticles.

The surface morphology of the Al-MNPs powder was observed by FE-SEM, which is shown in Fig. 3a. It is clearly seen that the electrodeposited iron oxide has particle morphology and the size of the observed particles is in the range of 20-30nm. The elemental analysis of the prepared nanoparticles was provided through energy-dispersive X-ray (EDX), which is presented in Fig. 3b. In this Figure, it is seen that the deposited NPs have the Fe, Mn and O elements with the percentages of composition 58.87%, 9.56% and 31.58%, respectively. With considering the fact that some of Fe^{3+} cations have

been substituted with Al^{3+} cations, as confirmed via XRD results, these values are very close to the percentage of Fe and O atoms in the Fe_3O_4 chemical formula i.e. 27.64% for O and 72.36% for Fe. These data clearly confirmed that the prepared iron oxide can be named as ~10% Al doped Fe_3O_4 nanoparticles.

The magnetic hysteresis loops and the enlarged low-field hysteresis for the prepared Al-MNPs sample are shown in Fig. 4. The magnetic data is also listed in Table 1.

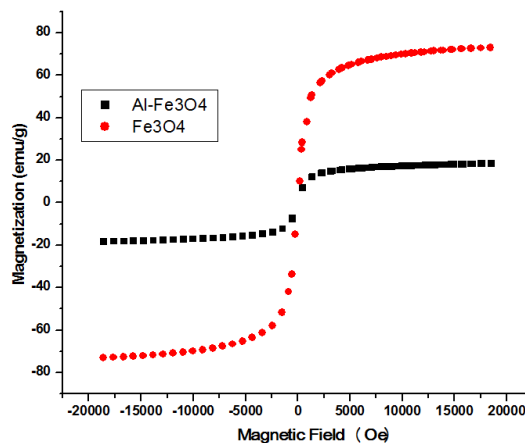


Figure 4. Hysteresis loops for the prepared undoped and Al doped magnetite nanoparticles.

Table 1. Magnetic data of the prepared Al doped magnetite nanoparticles

Sample name	Ms(emu/g)	Coercivity (Hci)G	Positive (Hci) G	Negative (Hci) G	Negative Mr(emu/g)	Positive Mr(emu/g)	Retentivity Mr(emu/g)
pure MNPs ^a	72.96	14.6	-41.87	-12.66	0.83	2.73	0.95
Al-MNPs	18.37	8.73	-2.23	-19.79	0.04	0.30	0.13

^a data has provided from Refs. [52,53].

The VSM profile of our powder exhibits complete S form as seen in Fig. 5 and no hysteresis is observed. These observations implicated that the prepared NPs have superparamagnetic nature. For comparison, the hysteresis profile of the undoped magnetite nanoparticles, from our previous works [52, 53], is also inserted in Fig. 5. It is clearly observable that the doped Fe_3O_4 NPs have better S form and it is expected that they exhibit better superparamagnetic data. For the prepared Al-MNPs, the magnetic data i.e. saturation magnetization (M_s), remanent magnetization or retentivity (Mr) and coercivity (H_{Ci}) are as follow (as listed in table 1); $M_s = 18.37 \text{ emu g}^{-1}$, $Mr=0.13 \text{ emu g}^{-1}$, positive $Mr = 0.30 \text{ emu g}^{-1}$, negative $Mr = 0.04 \text{ emu g}^{-1}$, $H_{Ci}=8.73 \text{ G}$, positive $H_{Ci}=-19.79$ and negative $H_{Ci}=-2.23\text{G}$. These data confirmed the superparamagnetic nature of the prepared Al-MNPs. Furthermore, these magnetic data are comparable with those of pure Fe_3O_4 NPs electro-synthesized at the sample electrochemical conditions. The magnetic data of pure MNPs have been reported to be [52,53]; $M_s = 72.96 \text{ emu g}^{-1}$, $Mr=0.95 \text{ emu g}^{-1}$, positive $Mr = 2.73 \text{ emu g}^{-1}$, negative $Mr = 0.83 \text{ emu g}^{-1}$, $H_{Ci}=14.61 \text{ G}$, positive $H_{Ci}=-12.66$ and negative $H_{Ci}=-41.87\text{G}$. Comparing these data indicates that the Al-MNPs

exhibit low saturation magnetization compared with pure MNPs, which is related to the low magnetization of Al atoms compared with Fe. However, Al-MNPs have smaller M_r and H_{Ci} values as compared with the pure MNPs, which proved their better superparamagnetic behavior. Hence, it can be concluded that doping MNPs with Al improves their superparamagnetic abilities.

3.2. Electrochemical studies

3.2.1. Cyclic voltammetry

The charge storage capacitance of the working electrode (WE) assembled from Al-MNPs was investigated by cyclic voltammetry (CV), and galvanostatic charge-discharge (GCD) techniques. Moreover, electrochemical impedance spectroscopy (EIS) was used to determine some of the electrochemical characters of the fabricated WE. All tests were carried out in a three-electrode cell containing 1M Na_2SO_3 electrolyte. The CVs of the prepared WE were obtained in a potential window of -1.0 to 0.1V vs. Ag/AgCl at the different scan rates, which is presented Fig. 6a.

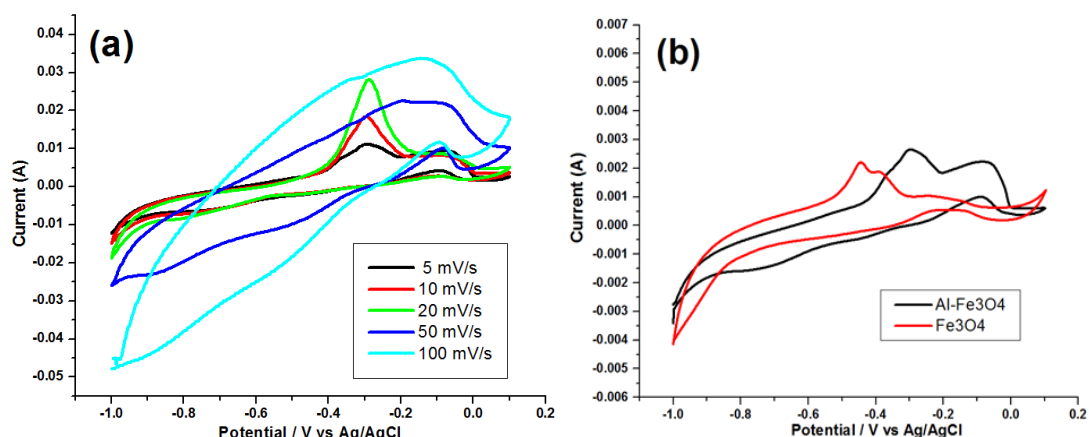


Figure 5. (a) CVs of Al doped magnetite nanoparticles at the various scan rates, (b) the calculated specific capacitances vs. scan rate.

The shapes of the CV profiles clearly reveal the pseudocapacitive performance of the fabricated WE. It has been reported that the charge storage of magnetite NPs in the Na_2SO_3 solution is based on both double layer and pseudocapacitance including the reduction/oxidation of specifically adsorbed sulfite anions on the iron oxide surface [31, 32]. As seen in Fig. 6a, the CVs of our WE exhibit small humps (i.e. redox peaks), which can be related to the electrochemical reactions of sulfite anions adsorbed onto the surface of magnetite NPs [34,54]:



The average SCs of the Al-MNPs electrode were obtained from the CVs in Fig. 6a by integrating the area under the current–potential curves [27]. Using Eq. (1), the SC values of the fabricated WE was determined to be 221.8, 204.7, 189.9, 145.6, 122.5, 102.7 and 88.3 F g^{-1} at the scan

rates of 2, 5, 10, 20, 50, 75 and 100 mV s^{-1} , respectively. The results show the proper super-capacitive performance of the Al doped magnetite NPs.

3.2.2. Charge-discharge tests

Galvanostatic charge-discharge (GCD) profiles were obtained at current densities of 0.2, 0.5, 1, 2, 3 and 5 A g^{-1} and are shown in Fig. 6a. The GCD profile of the made WE can be separated into two parts; the first part is a symmetric triangular form at potentials below $-0.4 \text{ V vs. Ag/AgCl}$, and second one is nonlinear dependency of potential at the potential of larger than $-0.4 \text{ V vs. Ag/AgCl}$. Former confirms the pure double-layer capacitance resulting from the behavior from the charge separation at the working electrode– Na_2SO_3 electrolyte interface. The latter indicates the typical pseudocapacitance behavior of the WE which is because of the faradic reactions (Eqs. 3 and 4).

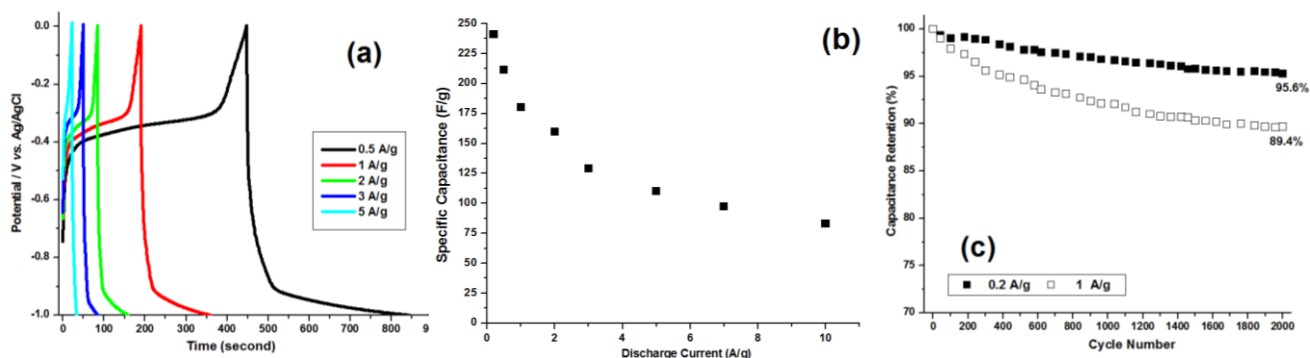


Figure 6. (a) GCD profiles of Al doped magnetite nanoparticles and (b) calculated SCs at the different current loads of 0.2 to 10 A g^{-1} , (c) capacity retention for 2000 charge-discharge cycling at the current load of 0.2 and 1 A g^{-1} .

The specific capacitance of the nano-particles was calculated using Eq. (2). The calculations revealed that the Fe_3O_4 nanoparticles are capable of delivering charge storages as high as 236.1 F g^{-1} at 0.2 A g^{-1} , 211.3 F g^{-1} at 0.5 A g^{-1} , 180.2 F g^{-1} at 1 A g^{-1} , 157.5 F g^{-1} at 2 A g^{-1} , 129.1 F g^{-1} at 3 A g^{-1} , 109.9 F g^{-1} at 5 A g^{-1} , 97.2 F g^{-1} at 7 A g^{-1} and 73.1 F g^{-1} at 10 A g^{-1} , respectively. These values are close to those calculated based on the CVs (Fig. 5b), confirming the excellent super-capacitive behaviour for the Al-MNPs. Furthermore, the charge storage performance of the prepared Al-MNPs are comparable with the data reported for the nanostructured pure magnetite electrodes in the literature (i.e. 185 F g^{-1} at 20 mV s^{-1} for magnetite NPs prepared by sol-gel [30], 207 F g^{-1} at 0.4 A g^{-1} for magnetite NPs prepared by ultrasonic synthesis [32], 157 F g^{-1} at 1 A g^{-1} for magnetite nanospheres prepared by PVP-assisted hydrothermal method [54], 170 F g^{-1} at 2 mV s^{-1} for magnetite thin film prepared by electroplating [55], 118.2 F g^{-1} at 0.6 A g^{-1} for magnetite thin film prepared by hydrothermal route [56] and 82 F g^{-1} at 1 A g^{-1} for magnetite thin film prepared by co-precipitation method [57]). Comparing these data with those delivered by our electrode implicated that the

supercapacitive performance iron oxide electrode is developed by Al doping. Also, cathodic deposition can be considered as an effective route for the preparation of high performance electrode materials based on metal doped iron oxide.

The cycle lives of the WEs were studied by GCD cycling (2000 cycles) in a 1M Na₂SO₃ electrolyte under a current density of 0.2 and 1 A/g. The specific capacitance of each cycle was calculated using Eq. (2) and, based on the resulted data, the cycle lives of the Al-MNPs was determined. Fig. 6 shows the cycling performance of the Al-MNPs during 2000 cycles at discharge current densities of 0.2 and 1 A g⁻¹. The specific capacity of the working electrodes maintain about 95.6% of its initial value after 2000 cycling at 0.2 A g⁻¹ as seen in Fig. 6c. Moreover, the WEs fabricated from the Al-MNPs keep about 89.4% of their initial capacity after 2000 continuous GCD cycle at a current load of 1 A g⁻¹. These data confirmed that the prepared Al-MNPs have suitable capacity retention during 2000 cycling in the 1M Na₂SO₃ electrolyte. The obtained results showed the excellent supercapacitive performance of the electro-synthesized Al-MNPs, as a result of their high surface area and ultra-fine size.

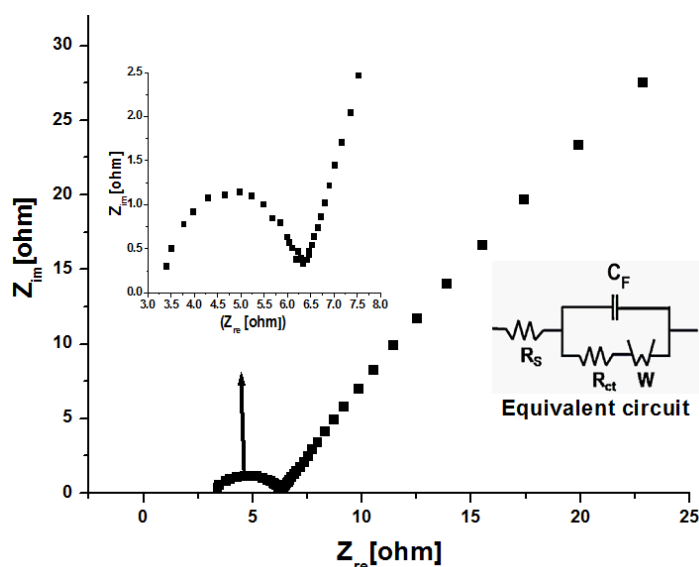


Figure 7. Nyquist plot of Al doped magnetite nanoparticles electrode with suggested equivalent circuit model.

3.2.3. EIS study

The WEs made of Al-MNPs were further studied through electrochemical impedance spectroscopy. Fig. 7 shows the Nyquist plot of the proposed working electrode, gotten in the frequency range of 10Hz to 100 kHz under open circuit potential. The Nyquist plot the WE is semicircular over the high frequency range, followed by a slanted line in the low frequency region. This plot can be fitted to an equivalent circuit comprising of an electrolyte resistance (R_s), a double layer capacitor (C_{dl}), a charge transfer resistance (R_{ct}), a Warburg element (Z_w) and a pseudocapacitor (C_p) as seen in the inset of Fig. 7. The equivalent series resistance (ESR) of the electrode was corresponded to its electroactive surface area (the combination of electrolyte accessible area and electrical conductivity).

The diameter of the semicircular section corresponds to the interfacial charge-transfer resistance (i.e. R_{ct}), also called the Faraday resistance. ESR and R_{ct} , which regularly inhibit the power density of a super-capacitor, were found to be 3.42Ω and 2.75Ω . These low ESR and Faraday resistance values indicate that the prepared Al-MNPs nanoparticles electrode can indicate remarkable supercapacitive performance. Additionally, the nearly ideal straight line along the imaginary axis at the lower frequencies indicates that the Al-MNPs have a low diffusion resistance. The resulted EIS proved the tremendous charge storage abilities detected from CV and GCD experiments.

4. CONCLUSION

In this work, Al-MNPs ultra-fine nanoparticles were deposited on surface of a cathode through cathodic electro-synthesis from mixed nitrate/chloride salt solutions, by controlling the applied current density in the cathodic deposition from mixed chloride/nitrate bath. The phase (i.e. pure magnetite), nanometer size (~ 20 nm) and Al content (10%wt.) of the electrodeposited iron oxide products were studied by XRD, FE-SEM and EDs analyses, respectively. Electrochemical studies revealed that the Al-MNPs offer excellent capacitive ability with delivering a specific capacitance values of 236.1 F g^{-1} at 0.2 A g^{-1} , 211.3 F g^{-1} at 0.5 A g^{-1} , 180.2 F g^{-1} at 1 A g^{-1} , 157.5 F g^{-1} at 2 A g^{-1} , 129.1 F g^{-1} at 3 A g^{-1} , 109.9 F g^{-1} at 5 A g^{-1} , 97.2 F g^{-1} at 7 A g^{-1} and 73.1 F g^{-1} at 10 A g^{-1} , respectively, indicating that the nano-material to be a promising candidate for super-capacitor applications.

ACKNOWLEDGEMENT

The authors are grateful to the Research Council of University of Tehran for the financial support of this work.

References

1. Y. Wang, Y. Song, and Y. Xia, *Chem. Soc. Rev.*, 45 (2016) 5925.
2. M. Aghazadeh, R. Ahmadi, D. Gharailou, M.R. , and P. Norouzi, *J. Mater. Sci.: Mater. Electron.*, 27 (2016) 8623.
3. M. Aghazadeh, *J. Appl. Electrochem.*, 42 (2012) 89.
4. M. Aghazadeh, A. Rashidy, and P. Norouzi, *Int. J. Electrochem. Sci.*, 11 (2016) 11016.
5. Y.X. Zhang, M. Huang, M. Kuang, C.P. Liu, J.L. Tan, M. Dong, Y. Yuan, X. Li Zhao, and Z. Wen, *Int. J. Electrochem. Sci.*, 8 (2013)1366
6. M. Aghazadeh, A. Rashidi, M.R. Ganjali, *Int. J. Electrochem. Sci.*, 11 (2016) 11002.
7. M. Aghazadeh, *J. Mater. Sci.: Mater. Electron.*, 28 (2017) 3108.
8. A. Barani, M. Aghazadeh, M.R. Ganjali, B. Sabour, A.A.M. Barmi, and S. Dalvand, *Mater. Sci. Semiconduct. Process.*, 23 (2014) 85.
9. B. Senthilkumar, R. KalaiSelvan, D. Meyrick, and M. Minakshi, *Int. J. Electrochem. Sci.*, 10 (2015)185.
10. S. Hassan, M. Suzuki, and A.A. ElMoneim, *Int. J. Electrochem. Sci.*, 9 (2014) 8340.
11. M. Aghazadeh, A. Bahrami-Samani, D. Gharailou, and M.G. Maragheh, M.R. Ganjali, *J. Mater. Sci.: Mater. Electron.*, 27 (2016) 11192.
12. H. R. Naderi, M. Reza Ganjali and P. Norouzi, *Int. J. Electrochem. Sci.*, 11 (2016) 4267.

13. M. Aghazadeh, M.G. Maragheh, M.R. Ganjali, P. Norouzi, D. Gharailou, and F. Faridbod, *J. Mater. Sci.: Mater. Electron.*, 27 (2016) 7707.
14. M. Aghazadeh, M.G. Maragheh, M.R. Ganjali, P. Norouzi, and F. Faridbod, *Appl. Surf. Sci.*, 364 (2016) 141.
15. M. Aghazadeh, M.G. Maragheh, M.R. Ganjali, and P. Norouzi, *RSC Advances*, 6 (2016) 10442.
16. C. Ma, S. Jian, J. Qiao, and J. Jung, *Int. J. Electrochem. Sci.*, 11 (2016) 10546.
17. M. Aghazadeh, A.A. Malek Barmi, D. Gharailou, M.H. Peyrovi, B. Sabour, and F. Najafi, *Appl. Surf. Sci.*, 283 (2013) 871.
18. Y. Li, L. Li, M. Cao, K. Dong, J.X. Wang, X.F. Zeng, J.F. Chen, and L. Shao, *Int. J. Electrochem. Sci.*, 12 (2017) 3432.
19. M. Aghazadeh, and S. Dalvand, *J. Electrochem. Soc.*, 161 (2014) D18.
20. M. Aghazadeh, H. Mohammad Shiri, and A.A. Malek Barmi, *Appl. Surf. Sci.*, 273 (2013) 237.
21. J. Talat Mehrabad, M. Aghazadeh, M.G. Maragheh, and M.R. Ganjali, *Mater. Lett.*, 184 (2016) 223.
22. M. Aghazadeh, M.R. Ganjali, and M.G. Maragheh, *Int. J. Electrochem. Sci.* 12 (2017) 5243.
23. Z. Yang, C. Fang, Y. Fang, Y. Zhou, and F. Zhu, *Int. J. Electrochem. Sci.*, 10 (2015) 1574.
24. J. Tizfahm, B. Safibonab, M. Aghazadeh, A. Majdabadi, B. Sabour, and S. Dalvand, *Colloids Surf. A.*, 443 (2014) 544.
25. M. Aghazadeh, A. Nozad Golikand, and M. Ghaemi, *Int. J. Hydrogen Energy*, 36 (2011) 8674.
26. M. Aghazadeh, B. Sabour, M.R. Ganjali, and S. Dalvand, *Appl. Surf. Sci.*, 313 (2014) 581.
27. M. Aghazadeh, I. Karimzadeh, and M.R. Ganjali, *J. Mater. Sci.: Mater. Electron.*, (2017) doi: 10.1007/s10854-017-7192-z
28. H. Gholipour-Ranjbar, M.R. Ganjali, P. Norouzi, and H.R. Naderi, *Ceram. Int.*, 42 (2016) 12097.
29. C. Wang, L. Wang, and K. Tang, *Int. J. Electrochem. Sci.*, 8 (2013) 4543.
30. E. Mitchell, R.K. Gupt, K. Mensah-Darkw, D. Kumar, K. Ramasamy, B.K. Gupta, and P. Kahol, *New J. Chem.*, 38 (2014) 4344.
31. V.D. Nithya , and N. Sabari Arul, *J. Power Source*, 327 (2016) 297.
32. L. Wang, H. Ji, S. Wang, L. Kong, X. Jiang, and G. Yang, *Nanoscale*, 5 (2013) 3793.
33. Y. Wang, Y. Ma, G. Guo, Y. Zhou, Y. Zhang, Y. Sun, and Y. Liu, *Int. J. Electrochem. Sci.*, 12 (2017) 2135.
34. V.D. Nithya, and N. Sabari Arul, *J. Mater. Chem. A.*, 4 (2016) 10767.
35. Z. Zhou, W. Xie, S. Li, X. Jiang, D. He, S. Peng, and F. Ma, *J. Solid State Electrochem.*, 19 (2015) 1211.
36. Y. Yang, J. Li, D. Chen, and J. Zhao, *ACS Appl. Mater. Interfaces*, 8 (2016) 26730.
37. S. Chen, R. Zhou, Y. Chen, Y. Fu, P. Li, Y. Song, and L. Wang, *J. Nanopart. Res.*, 19 (2017) 127.
38. Y.Z. Wu, M. Chen, X.H. Yan, J. Ren, Y. Dai, J.J. Wang, J.M. Pan, Y.P. Wang, and X.N. Cheng, *Mater.Lett.*, 198 (2017) 114.
39. H. Fan, R.Niu, J. Duan, W. Liu, and W. Shen, *ACS Appl. Mater. Interfaces*, 8 (2016) 19475.
40. J. Shabani Shayeh, A. Ehsani, M. R. Ganjali, P. Norouzi, B. Jaleh, *Applied Surface Science*, 353 (2015) 594.
41. X. Yang, J. Kan, F. Zhang, M. Zhu, and Z. Li, *J.Inorg. Org. Polym. Mater.*, 27 (2017) 542.
42. X. Tang, R. Jia, T. Zhai, and H. Xia, *ACS Appl. Mater. Interfaces*, 7 (2015) 27518.
43. T. Xia, X. Xu, J. Wang, C. Xu, F. Meng, Z. Shi, J. Lian, and J. M. Bassat, *Electrochim. Acta.*, 160 (2015) 114.
44. W.M. Zhang, X.L. Wu, J.S. Hu, Y.G. Guo, and L.J. Wan, *Adv. Funct. Mater.*, 18 (2008) 3941.
45. X. Xia, Y. Zhang, D. Chao, C. Guan, Y. Zhang, L. Li, X. Ge, I.M. Bacho, J. Tu, and H.J. Fan, *Nanoscale*, 6 (2014) 5008.
46. I. Karimzadeh, M. Aghazadeh, M.R. Ganjali, P. Norouzi, and T. Doroudi, *Mater. Lett.*, 189 (2017) 290.
47. I. Karimzadeh, H.R. Dizaji, and M. Aghazadeh, *Mater. Res. Express*, 3 (2016) 095022.
48. I. Karimzadeh, M. Aghazadeh, M.R. Ganjali, and T. Dourudi, *Curr. Nanosci.*, 13 (2017) 167.

49. I. Karimzadeh, M. Aghazadeh, T. Doroudi, M.R. Ganjali, and P.H. Kolivand, *Adv. Phys. Chem.*, 2017 (2017) 7.
50. I. Karimzadeh, M. Aghazadeh, T. Doroudi, M.R. Ganjali, and D. Gharailou, *J. Cluster Sci.*, 12 (2017) 3231.
51. L.G. Beka, X. Li, and W. Liu, *J. Mater. Sci.: Mater. Electron.*, 27 (2016) 10894.
52. I. Karimzadeh, H.R. Dizaji, and M. Aghazadeh, *J. Magn. Magn. Mater.*, 416 (2016) 81.
53. M. Aghazadeh, I. Karimzadeh, M.R. Ganjali, and M. Mohebi Morad, *Mater. Lett.*, 196, 392 (2017)
54. K. Bhattacharya, and P. Deb, *Dalton Trans.*, 44 (2015) 9221.
55. S.Y. Wang, K.C. Ho, S.L. Kuo and N.L. Wu, *J. Electrochem. Soc.*, 153 (2006) A75.
56. J. Chen, K. Huang, and S. Liu, *Electrochim. Acta*, 55 (2009) 1.
57. S.C. Pang, W.H. Khoh, and S.F. Chin, *J. Mater. Sci.*, 45 (2010) 5598.

© 2017 The Authors. Published by ESG (www.electrochemsci.org). This article is an open access article distributed under the terms and conditions of the Creative Commons Attribution license (<http://creativecommons.org/licenses/by/4.0/>).